International Journal of Computational Methods
Vol. 8, No. 1 (2011) 77–90

DOI: 10.1142/S0219876211002435

LIMIT CYCLE OSCILLATION PREDICTION AND CONTROL DESIGN METHOD FOR AEROELASTIC SYSTEM BASED ON NEW NONLINEAR REDUCED ORDER MODEL

CHEN GANG, LI YUE-MING and YAN GUI-RONG
MOE Key Laboratory for Strength & Vibration
College of Aerospace, Xi'an Jiaotong University
Xi'an, PRC, 710049

Received 2 May 2010
Accepted 14 June 2010

When the amplitude of the oscillation of the unsteady flow is large or there is large perturbation relative to the mean background flow, the traditional proper orthogonal decomposition/reduced order model (POD/ROM) based on linearized time or frequency domain small disturbance solvers cannot capture the main nonlinear features well such as limit cycle oscillation (LCO), which is very dangerous for the structure. Therefore, the traditional linear ROMs are not good enough for limit cycles prediction and active control law design. A new nonlinear ROM based on dynamically nonlinear flow equation NPOD/ROM was investigated. The nonlinear second-order snapshot equation in time domain for POD basis construction is obtained from the Taylor series expansion of the flow solver. The simulation results indicate that the NPOD/ROM can capture LCO very well and is also very convenient for active control law design, while the traditional POD/ROM lose effectiveness.

Keywords: Reduced order model; limit cycle oscillation; proper orthogonal decomposition; aeroelasticity; active control.

1. Introduction

With the development of computational aeroelasticity, the aeroelastic response can be accurately predicted by the high-fidelity physics-based mathematical model such as CFD/CSD couple solver. However, the computation cost is too large for these high-fidelity methods to be applied to the multidisciplinary conception design in which there are lots of iterations. Unlike high-fidelity couple solver, reduced order model (ROM) seeks to construct a simple mathematical representation model, which captures the dominate behavior of aeroelastic system and can be convenient to use in conception design, control, and data-driven systems [Lucia *et al.* (2004)].

Many approaches for constructing linear flow and aeroelastic ROMs have been developed and shown to produce good numerical results that compare well with

high-fidelity nonlinear solver. Among these approaches, the ROM based on proper orthogonal decomposition (POD/ROM) is recently becoming the most popular. For example, the POD/ROM was successfully applied to the CFD-based aeroelastic analysis of airfoil [Thomas *et al.* (2004)], wing [Thomas *et al.* (2003)], and full aircraft [Lieu *et al.* (2006)], especially in flutter prediction [Thomas *et al.* (2003); Lieu *et al.* (2006); Lai and Tsai (2008)]. These ROMs are typically constructed based on the linearized time or frequency domain small disturbance solvers that are dynamically linearized about some nonlinear stationary background flow state. Most aeroelastic phenomena such as flutter and gust response can be deal with these ROMs based on dynamically linearization equation. However, unfortunately, some important strong nonlinear dynamics with large structure deformation cannot be simulated by the small disturbance solvers, for example, limit cycle oscillation (LCO), which is one of the major nonlinear dynamic aeroelastic unstable phenomena and very dangerous to aircraft structure. Because of the poor performance in LCO prediction, the POD/ROM is scarcely used in active control law design for LCO.

For modeling the cases where the amplitude of the unsteady flow oscillation is large or large changes occur in the mean background flow, the ROMs for dynamically nonlinear solvers are required, for the linearized time or frequency domain small disturbance solvers cannot capture the main nonlinear features [Dowell *et al.* (2003); Hu and Dowell (2008)]. Such ROMs are essential for matched point flutter onset analysis as well as nonlinear LCO analysis. The low fidelity model cannot predict the strong aerodynamic nonlinearity very well, so the design of control law for LCO is a tedious work that requires the help of high fidelity tool such as CFD/CSD couple solver. There are seldom successful reports for the traditional time-domain POD/ROM to predict LCO generate by the aerodynamic nonlinearity. On behalf of the harmonics including some nonlinear flow information, the first-order frequency-domain HB/POD solver developed by Dowell [Thomas *et al.* (2004); Dowell *et al.* (2004)] can capture LCO very well in some instances; however, there are still obvious errors in other instances far away from the frequency where the ROM was created. Recently, Badcock had put forward a fully nonlinear ROM construction method based on bifurcation theory, which is an excellent fully nonlinear ROM and can predict LCO very well [Badcock and Woodgate (2007)]. Badcock's bifurcation ROM is a new type of ROM, not belong to POD/ROM.

We will develop a new dynamically nonlinear solver-based POD/ROM, or NPOD/ROM, which will enable the rapid modeling of nonlinear unsteady aerodynamic flows and the associated fluid forces, especially for the LCO prediction and control. The main idea of NPOD/ROM is to extend the conventional dynamically linear POD snapshot equation to dynamically nonlinear snapshot equation by second-order Taylor serials expansion in time domain. It means that the traditional POD/ROM is first-order model, while the NPOD/ROM is second-order model.

2. The POD Algorithm

For one series data $\{x^k\}x^k \in \mathbb{C}^n$, which is called snapshot, construct an m-dimension proper orthogonal subspace $\Psi \in \Re^{n\times m}$ to minimize the mapping errors from $\{x^k\}$ to Ψ:

$$G = \min_{\Phi} \sum_{k=1}^{m} \|x^k - \Phi\Phi^H x^k\| = \sum_{k=1}^{m} \|x^k - \Psi\Psi^H x^k\|, \quad \Phi^H\Phi = I. \tag{1}$$

It equals to:

$$H = \max_{\Phi} \sum_{k=1}^{m} \frac{\langle (x^k, \Phi)^2 \rangle}{\|\Phi\|^2} = \sum_{k=1}^{m} \frac{\langle (x^k, \Psi)^2 \rangle}{\|\Psi\|^2}, \quad \Phi^H\Phi = I \tag{2}$$

$\langle\cdot\rangle$ is mean value operator, which can be neglected if the snapshot matrix is computed by numerical method, and $(\cdot,\cdot)$ is inner product. The constraint optimization problem of Eq. (2) can be transformed into Lagarange equation:

$$J(\Phi) = \sum_{k=1}^{m} (x^k, \Phi)^2 - \lambda(\|\Phi\| - 1). \tag{3}$$

Solve the partial derivative objective function $J(\Phi)$ to Φ, and there is:

$$\frac{d}{d\Phi} J(\Phi) = 2XX^H\Phi - 2\lambda\Phi. \tag{4}$$

$X = \{x^1 \ x^2 \ \cdots \ x^m\}$ is the snapshot matrix. Let Eq. (4) equal zero:

$$(XX^H - \lambda I)\Psi = 0. \tag{5}$$

Equation (5) is a real symmetry eigenvalue problem about POD kernel $K = XX^H$. Considering that XX^H and X^HX have the same eigenvalue, we can obtain Ψ from the follow lower m-dimension problem:

$$\begin{cases} X^HXV = V\Lambda \\ \Psi = XV\Lambda^{-1/2}. \end{cases} \tag{6}$$

$\Psi = [\psi_1 \ \psi_2 \ \cdots \ \psi_m], \Lambda = \mathrm{diag}(\lambda_1 \ \lambda_2 \cdots \lambda_m), \lambda_1 \geq \lambda_2 \geq \cdots \geq \lambda_m$. Truncate Ψ to r-order vector $\Psi_r = [\psi_1 \ \psi_2 \cdots \psi_r]$, the n-order full system $x^{n\times 1}$ can be reduced to an r-order system:

$$x^{n\times 1} = \Psi_r \xi^{r\times 1}. \tag{7}$$

3. NPOD/ROM Method

3.1. *Aeroelastic equation*

The full-coupled nonlinear aeroelastic equation decentralized by finite volume method for flow and finite element method for structure is:

$$\frac{d\mathbf{A}(\mathbf{u}, \dot{\mathbf{u}})\mathbf{w}}{dt} + \mathbf{R}(\mathbf{w}, \mathbf{u}, \dot{\mathbf{u}}) = 0 \tag{8}$$

$$Mv_{,t} + f^{\mathrm{int}}(u, v) = f^{\mathrm{ext}}(u, w). \tag{9}$$

For the flow equation, $\vec{w}$ is conservative flow field value including flow velocity, flow density, and enthalpy. R is flux value, A is fluid cell volume, $\vec{u}$ is structure general displacement, and $\vec{v}$ is structure general displacement derivatives. For structure equation, M is mass matrix, f^{int} is structure inner force, and f^{ext} is the aerodynamic loads acting on the structure.

3.2. *Dynamically nonlinear flow equation*

3.2.1. *Nonlinear snapshot equation*

The first step for reducing the flow system is to compute the values of the operators $(\cdot,\cdot)$ and $\langle\cdot\rangle$, or the covariant matrix of the unsteady flow values, which are the so-called snapshots. For the FVM-decentralized NS equation, at the convergent steady flow $(\mathbf{w}_0, \mathbf{u}_0, \dot{\mathbf{u}}_0)$, there are:

$$\frac{d\mathbf{A}(\mathbf{u}_0, \dot{\mathbf{u}}_0)\mathbf{w}_0}{dt} = \mathbf{R}(\mathbf{w}_0, \mathbf{u}_0, \dot{\mathbf{u}}_0) = 0$$
$$\mathbf{R}(\mathbf{w}, \mathbf{u}, \dot{\mathbf{u}}) = 0, \quad \dot{\mathbf{w}}_0 = 0, \quad \mathbf{u}_0 = 0, \quad \dot{\mathbf{u}}_0 = 0, \quad \ddot{\mathbf{u}}_0 = 0.$$

Suppose $(\delta\mathbf{w}, \delta\mathbf{u}, \delta\dot{\mathbf{u}})$ is the flow perturbation around the nonlinear steady background flow $(\mathbf{w}_0, \mathbf{u}_0, \dot{\mathbf{u}}_0)$ and then expand the flow Eq. (8) at $(\mathbf{w}_0, \mathbf{u}_0, \dot{\mathbf{u}}_0)$ by the Taylor serials. The first item of Eq. (8) is:

$$\mathbf{A}(\mathbf{u}, \dot{\mathbf{u}})\dot{\mathbf{w}} + \left(\mathbf{w}\frac{\partial A}{\partial \mathbf{u}}\right) \cdot \dot{\mathbf{u}} + \left(\mathbf{w}\frac{\partial A}{\partial \dot{\mathbf{u}}}\right) \cdot \ddot{\mathbf{u}} = \mathbf{A}(\mathbf{u}, \dot{\mathbf{u}})\dot{\mathbf{w}} + \mathbf{E} \cdot \dot{\mathbf{u}} + \mathbf{D} \cdot \ddot{\mathbf{u}}. \tag{10}$$

Considering that the Geometry Conservation Law of FVM method is only with second-order accuracy, the third-order effect, or the gird acceleration effect can be neglect. Therefore, the last item of Eq. (10) is neglected. By retaining the second-order items of Taylor serials of the above equation, we obtain:

$$\begin{aligned}
\mathbf{A}(\mathbf{u}, \dot{\mathbf{u}})\dot{\mathbf{w}} &= A(\mathbf{u}_0 + \delta\mathbf{u}, \dot{\mathbf{u}}_0 + \delta\dot{\mathbf{u}})(\dot{\mathbf{w}}_0 + \delta\dot{\mathbf{w}}) = \mathbf{A}(\mathbf{u}_0 + \delta\mathbf{u}, \dot{\mathbf{u}}_0 + \delta\dot{\mathbf{u}})\delta\dot{\mathbf{w}} \\
&= \left[\mathbf{A}(\mathbf{u}_0, \mathbf{o}) + \left(\frac{\partial A}{\partial \mathbf{u}}\right)_0 \delta\mathbf{u} + \left(\frac{\partial A}{\partial \dot{\mathbf{u}}}\right)_0 \delta\dot{\mathbf{u}}\right] \delta\dot{\mathbf{w}} \qquad (11) \\
\mathbf{E}\dot{\mathbf{u}} &= \mathbf{E}_0 \cdot \dot{\mathbf{u}}_0 + \mathbf{E}_0 \cdot \delta\dot{\mathbf{u}} + \left(\frac{\partial \mathbf{E}}{\partial \mathbf{w}}\delta\mathbf{w} + \frac{\partial \mathbf{E}}{\partial \mathbf{u}}\delta\mathbf{u} + \frac{\partial \mathbf{E}}{\partial \dot{\mathbf{u}}}\delta\dot{\mathbf{u}}\right)_0 \cdot \dot{\mathbf{u}}_0 \\
&\quad + \left(\frac{\partial \mathbf{E}}{\partial \mathbf{w}}\delta\mathbf{w} + \frac{\partial \mathbf{E}}{\partial \mathbf{u}}\delta\mathbf{u} + \frac{\partial \mathbf{E}}{\partial \dot{\mathbf{u}}}\delta\dot{\mathbf{u}}\right)_0 \delta\dot{\mathbf{u}} \\
&= \mathbf{E}_0 \cdot \delta\dot{\mathbf{u}} + \left(\frac{\partial A}{\partial \mathbf{u}}\delta\mathbf{w} + \mathbf{w}\frac{\partial^2 \mathbf{A}}{\partial \mathbf{u}^2}\delta^2\mathbf{u} + \mathbf{w}\frac{\partial^2 \mathbf{A}}{\partial \mathbf{u}\partial \dot{\mathbf{u}}}\delta\dot{\mathbf{u}}\delta\mathbf{u}\right)_0 \delta\dot{\mathbf{u}} \\
&= \mathbf{w}_0\frac{\partial A}{\partial \mathbf{u}}(\mathbf{u}_0) \cdot \delta\dot{\mathbf{u}} + \left(\frac{\partial A}{\partial \mathbf{u}}\right)_0 \delta\mathbf{w}\delta\dot{\mathbf{u}}. \qquad (12)
\end{aligned}$$

Expand the second item of equation and neglect the third-order item, there is:

$$\begin{aligned}\mathbf{R}(\mathbf{w},\mathbf{u},\dot{\mathbf{u}}) &= \mathbf{R}(\mathbf{w}_0,\mathbf{u}_0,\dot{\mathbf{u}}_0) + \left(\frac{\partial \mathbf{R}}{\partial \mathbf{w}}\right)_0 \delta\mathbf{w} + \left(\frac{\partial \mathbf{R}}{\partial \mathbf{u}}\right)_0 \delta\mathbf{u} + \left(\frac{\partial \mathbf{R}}{\partial \dot{\mathbf{u}}}\right)_0 \delta\dot{\mathbf{u}} \\ &\quad + \frac{1}{2!}\left(\frac{\partial}{\partial \mathbf{w}}\delta\mathbf{w} + \frac{\partial}{\partial \mathbf{u}}\delta\mathbf{u} + \frac{\partial}{\partial \dot{\mathbf{u}}}\delta\dot{\mathbf{u}}\right)_0^2 \mathbf{R}(\mathbf{w},\mathbf{u},\dot{\mathbf{u}}) \\ &= \frac{1}{2}\left(\frac{\partial^2 \mathbf{R}}{\partial^2 \mathbf{w}}\right)_0 \delta^2\mathbf{w} + \left[\left(\frac{\partial \mathbf{R}}{\partial \mathbf{w}}\right)_0 + \left(\frac{\partial^2 \mathbf{R}}{\partial \mathbf{w}\partial \mathbf{u}}\right)_0 \delta\mathbf{u} + \left(\frac{\partial^2 \mathbf{R}}{\partial \mathbf{w}\partial \dot{\mathbf{u}}}\right)_0 \delta\dot{\mathbf{u}}\right]\delta\mathbf{w} \\ &\quad + \frac{1}{2}\left(\frac{\partial^2 \mathbf{R}}{\partial^2 \mathbf{u}}\right)_0 \delta^2\mathbf{u} + \frac{1}{2}\left(\frac{\partial^2 \mathbf{R}}{\partial^2 \mathbf{w}}\right)_0 \delta^2\dot{\mathbf{u}} \\ &\quad + \left(\frac{\partial^2 \mathbf{R}}{\partial \mathbf{u}\partial \dot{\mathbf{u}}}\right)_0 \delta\mathbf{u}\delta\dot{\mathbf{u}} + \left(\frac{\partial \mathbf{R}}{\partial \mathbf{u}}\right)_0 \delta\mathbf{u} + \left(\frac{\partial \mathbf{R}}{\partial \dot{\mathbf{u}}}\right)_0 \delta\dot{\mathbf{u}}. \end{aligned} \tag{13}$$

The total second-order Taylor serials or the discrete NS equation can be rearrange by $\delta\mathbf{w}$:

$$\begin{aligned}&\left[A(\mathbf{u}_0,\mathbf{o}) + \left(\frac{\partial A}{\partial \mathbf{u}}\right)_0 \delta\mathbf{u} + \left(\frac{\partial A}{\partial \dot{\mathbf{u}}}\right)_0 \delta\dot{\mathbf{u}}\right]\delta\dot{\mathbf{w}} + \frac{1}{2}\left(\frac{\partial^2 \mathbf{R}}{\partial^2 \mathbf{w}}\right)_0 \delta^2\mathbf{w} \\ &\quad + \left[\left(\frac{\partial \mathbf{R}}{\partial \mathbf{w}}\right)_0 + \left(\frac{\partial A}{\partial \mathbf{u}}\right)_0 \delta\dot{\mathbf{u}} + \left(\frac{\partial^2 \mathbf{R}}{\partial \mathbf{w}\partial \mathbf{u}}\right)_0 \delta\mathbf{u} + \left(\frac{\partial^2 \mathbf{R}}{\partial \mathbf{w}\partial \dot{\mathbf{u}}}\right)_0 \delta\dot{\mathbf{u}}\right]\delta\mathbf{w} \\ &\quad + \frac{1}{2}\left(\frac{\partial^2 \mathbf{R}}{\partial^2 \mathbf{u}}\right)_0 \delta^2\mathbf{u} + \frac{1}{2}\left(\frac{\partial^2 \mathbf{R}}{\partial^2 \dot{\mathbf{u}}}\right)_0 \delta^2\dot{\mathbf{u}} + \left(\frac{\partial^2 \mathbf{R}}{\partial \mathbf{u}\partial \dot{\mathbf{u}}}\right)_0 \delta\mathbf{u}\delta\dot{\mathbf{u}} \\ &\quad + \left(\frac{\partial \mathbf{R}}{\partial \mathbf{u}}\right)_0 \delta\mathbf{u} + \left[\mathbf{w}_0 \frac{\partial A}{\partial \mathbf{u}}(\mathbf{u}_0) + \left(\frac{\partial \mathbf{R}}{\partial \dot{\mathbf{u}}}\right)_0\right]\delta\dot{\mathbf{u}} = 0. \end{aligned} \tag{14}$$

The accuracy of the spatial discretization scheme is not more than third order, and the derivatives of flux to grid displacement and velocity are bigger than second-order partial derivatives. The nondimensional $\delta\mathbf{u}$ and $\delta\dot{\mathbf{u}}$ are also smaller than one. Therefore, the second-order items $(\frac{\partial^2 \mathbf{R}}{\partial^2 \mathbf{u}})_0\delta^2\mathbf{u}$, $(\frac{\partial^2 \mathbf{R}}{\partial^2 \dot{\mathbf{u}}})_0\delta^2\dot{\mathbf{u}}$, $(\frac{\partial^2 \mathbf{R}}{\partial \mathbf{u}\partial \dot{\mathbf{u}}})_0\delta\mathbf{u}\delta\dot{\mathbf{u}}$ are lesser than the first-order items of $\delta\mathbf{u}$ and $\delta\dot{\mathbf{u}}$, and they can be neglected. Finally, we obtain the dynamically nonlinear POD snapshot equation such as:

$$\begin{aligned}&\mathbf{A}_1\delta\dot{\mathbf{w}} + \mathbf{B}_1\delta^2\mathbf{w} + \mathbf{H}_1\delta\mathbf{w} + \mathbf{G}_1\delta\mathbf{u} + (\mathbf{C}_1 + \mathbf{E}_1)\delta\dot{\mathbf{u}} = 0 \\ &\mathbf{A}_1 = \mathbf{A}(\mathbf{u}_0,\mathbf{o}) + \left(\frac{\partial A}{\partial \mathbf{u}}\right)_0 \delta\mathbf{u} + \left(\frac{\partial A}{\partial \dot{\mathbf{u}}}\right)_0 \delta\dot{\mathbf{u}} \\ &\mathbf{B}_1 = \frac{1}{2}\left(\frac{\partial^2 \mathbf{R}}{\partial^2 \mathbf{w}}\right)_0, \\ &\mathbf{H}_1 = \left(\frac{\partial \mathbf{R}}{\partial \mathbf{w}}\right)_0 + \left(\frac{\partial A}{\partial \mathbf{u}}\right)_0 \delta\dot{\mathbf{u}} + \left(\frac{\partial^2 \mathbf{R}}{\partial \mathbf{w}\partial \mathbf{u}}\right)_0 \delta\mathbf{u} + \left(\frac{\partial^2 \mathbf{R}}{\partial \mathbf{w}\partial \dot{\mathbf{u}}}\right)_0 \delta\dot{\mathbf{u}}. \end{aligned} \tag{15}$$

The partial derivatives, including the first and second Jacobian terms, should be computed previously according to the background flow. In order to ensure the accuracy of the Jacobian terms, the automatic differentiation tool was used, which is as good as analytical method. The inputs are $\delta\mathbf{u}$ and $\delta\dot{\mathbf{u}}$, and the output is $\delta\mathbf{w}$, which can be solved by the Newton–Raphson technique. $\delta\mathbf{w}$ is the nonlinear snapshot required for ROM construction.

3.2.2. *NPOD/ROM for aeroelastic system*

Suppose the snapshot matrix is W and the POD kernel matrix is $R = WW^T$. Use the POD algorithm to obtain an r-dimension proper orthogonal subspace Ψ_r which can be considered as the fluid mode, then project Eq. (8) to Ψ_r, and we can get the nonlinear NPOD/ROM for aeroelastic system:

$$\begin{aligned} &\mathbf{A}_1\Psi_r\delta\dot{\mathbf{w}}_r + \mathbf{B}_1\Psi_r^2\delta^2\mathbf{w}_r + \mathbf{H}_1\Psi_r\delta\mathbf{w}_r + \mathbf{G}_1\delta\mathbf{u} + (\mathbf{C}_1 + \mathbf{E}_1)\delta\dot{\mathbf{u}} = \mathbf{0} \\ &\mathrm{M}\ddot{\mathbf{u}} + \mathbf{C}\dot{\mathbf{u}} + \mathbf{K}_s\mathbf{u} - q_\infty\mathbf{P}\Psi_r\delta\mathbf{w}_r = \mathbf{0}, \end{aligned} \tag{16}$$

where $P = \frac{\partial f^{\text{ext}}}{\partial w}(u_0, w_0)$, $K_s = K_0 - \frac{\partial f^{\text{ext}}}{\partial u}(u_0, w_0)$. The s is the order of the structure equation, which can be reduced by structure modes. The order of the system (16) is just $2s + r$ and it is smaller than the original system. It is very convenient to analyze the stability and the time response of the system from the NPOD/ROM. It is simple and efficient than CFD/CSD coupled computation.

3.3. *Traditional POD/ROM*

Retain the first-order items of Eq. (15), and the full-order dynamically linearized snapshot equation can be obtained:

$$A_0\delta\dot{\mathbf{w}} + \mathbf{H}\delta\mathbf{w} + \mathbf{G}\delta\mathbf{u} + (\mathbf{C} + \mathbf{E})\delta\dot{\mathbf{u}} = 0 \tag{17}$$

$$\begin{aligned} \mathbf{H} &= \frac{\partial\mathbf{R}}{\partial\mathbf{w}}(\mathbf{w}_0, \mathbf{u}_0, \dot{\mathbf{u}}_0) \\ \mathbf{G} &= \frac{\partial\mathbf{R}}{\partial\mathbf{u}}(\mathbf{w}_0, \mathbf{u}_0, \dot{\mathbf{u}}_0) \\ \mathbf{C} &= \frac{\partial\mathbf{R}}{\partial\dot{\mathbf{u}}}(\mathbf{w}_0, \mathbf{u}_0, \dot{\mathbf{u}}_0) \\ \mathbf{E} &= \mathbf{w}_0\frac{\partial A}{\partial\mathbf{u}}(\mathbf{u}_0). \end{aligned} \tag{18}$$

The linearization fluid Eq. (17) can be transformed into the state space equation:

$$\begin{cases} \dot{w} = Aw + B[v\ u]^T \\ F = Cw. \end{cases} \tag{19}$$

$A = -A_0^{-1}H$, $B = -A_0^{-1}[E + C\ G]$, $C = P$. Use the algorithm in Sec. 2 to obtain r-dimension proper orthogonal subspace Ψ_r, project the Eq. (13) into Ψ_r and we

can obtain the reduced fluid model:

$$\begin{cases} \dot{w}_r = \Psi_r^T A \Psi_r w_r + \Psi_r^T B y \\ F = P \Psi_r w_r. \end{cases} \tag{20}$$

Replace Eq. (20) into Eq. (9), the traditional time-domain POD/ROM of aeroelastic system can be represented as follows:

$$\begin{bmatrix} \dot{w}_r \\ \dot{v} \\ \dot{u} \end{bmatrix} = \begin{bmatrix} -\Psi_r^T A_0^{-1} H \Psi_r & -\Psi_r^T A_0^{-1}(E+C) & -\Psi_r^T A_0^{-1} G \\ \frac{1}{2}\rho_\infty V_\infty^2 \bar{M}^{-1} P \Psi_r & -\bar{M}^{-1}\bar{C} & -\bar{M}^{-1}\bar{K}_S \\ 0 & I & 0 \end{bmatrix} \begin{bmatrix} w_r \\ v \\ u \end{bmatrix}. \tag{21}$$

As it can be seen, the traditional time-domain POD/ROM is just one special case of the NPOD/ROM.

4. Numerical Validation

4.1. *NLR 7301 airfoil aeroelastic model*

As a demonstration for the efficiency of the new NPOD/ROM, the NLR 7301 airfoil section aeroelastic model with the pitch and plunge movement was selected, which was tested extensively in wind tunnel by Schewe [Dietz *et al.* (2004)] and numerical simulated by Dowell [Thomas *et al.* (2004)]. The detail of the model parameters can be founded in their references. Transonic two-degree-of-freedom aeroelastic experimental studies were conducted for various Mach numbers and angles of attack and, and LCO was observed in some instances.

4.2. *Snapshots comparison between linearization and nonlinear equation*

The 400×100 O-type mesh was used for aerodynamic computation. At $\mathrm{Ma} = 0.76$, $\alpha = 0°$, $h = 0$, $V^* = 0.37$, the unsteady lift coefficient responses of different fidelity models were observed. Figure 1 plots the lift coefficient response of CFD, linear, and nonlinear snapshot equations at airfoil pitch vibration movement with a very little amplitude. The results of different model are very closely. It verifies once again that the linear model has the enough accuracy to predict the unsteady aerodynamics at the case of small disturbance [Dowell *et al.* (2003)]. It also clearly points out the essentials why the conventional or first-order POD/ROM can represent the traditional aeroelastic dynamics very well such as flutter and gust response, because they are still small perturbation relative to the reference steady flow.

Then enlarge the amplitude of vibration by 10 times and observe the unsteady aerodynamic response again. Figure 2 is the unsteady lift coefficient response of CFD, linear, and nonlinear snapshot equations. It is seen clearly that the linearization snapshot equation has obvious errors both in amplitude and in frequency, while the nonlinear snapshot equation still shows good performance.

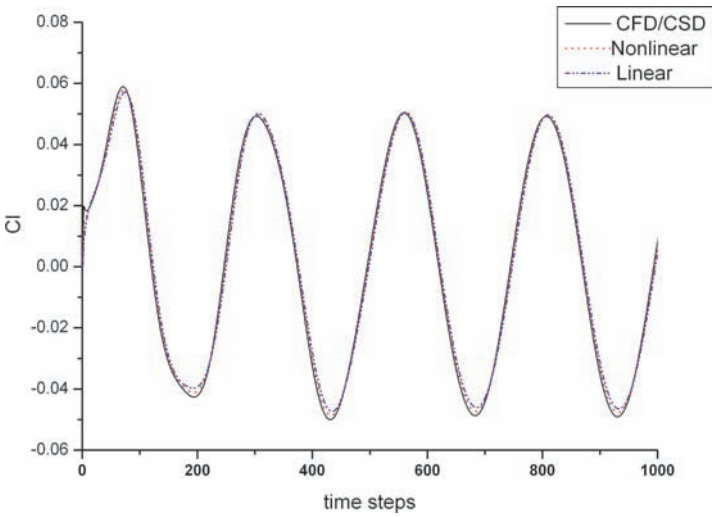

Fig. 1. Lift response (little disturbance).

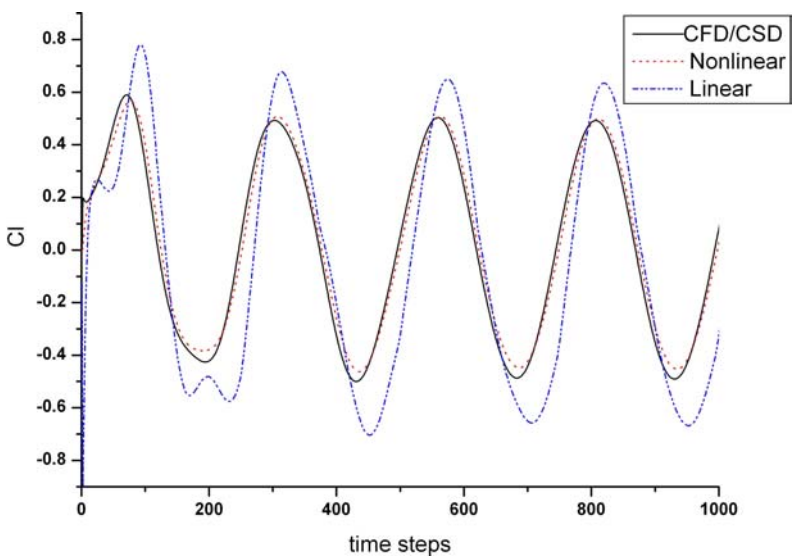

Fig. 2. Lift response (large disturbance).

4.3. *LCO prediction*

Use the Eqs. (15) and (17) to solve the snapshots with the time step of 5×10^{-5} s and obtain 200-step response from Dirac triangle impulse function for each mode displacement and mode velocity for each structure mode movements at the condition of Ma = 0.75, $\alpha = 0°$. Then, 100-order POD/ROM and NPOD/ROM for the aeroelastic system are constructed. The number of the ROM order was selected

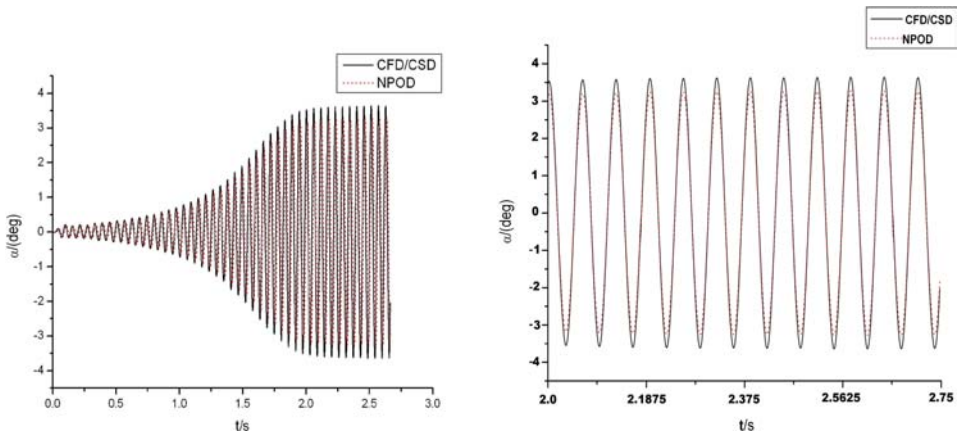

Fig. 3. Pitch movement predicted by NPOD vs. CFD/CSD solver.

according to the accuracy of the ROM for the flutter prediction. We find that the 100-order POD/ROM was good enough to do that.

We hope to meet the LCO at the reduced velocity $V^* = 0.376$, which is above the flutter point. In this case, the conventional time-domain linear POD/ROM lose its way while the NPOD/ROM catches the LCO. Figure 3 is the pitch responses of LCO predicted by the NPOD/ROM and the direct CFD/CSD couple solver. Figure 4 is the plunge movement of the LCO. The right of the pictures is the local zoom map. The amplitude error of the LCO predicted by the NPOD/ROM is less than 8% of those by the CFD/CSD solver. The LCO is very close to the Tang's results [Thomas *et al.* (2008)], which were computed by the CFL3D solver. The consistent response shows the capability and accuracy of NPOD/ROM for LCO prediction. The unsteady flow field after the airfoil run into LCO also was reconstructed by the 100-order NPOD/ROM, and it was founded that the reconstructed flow field was

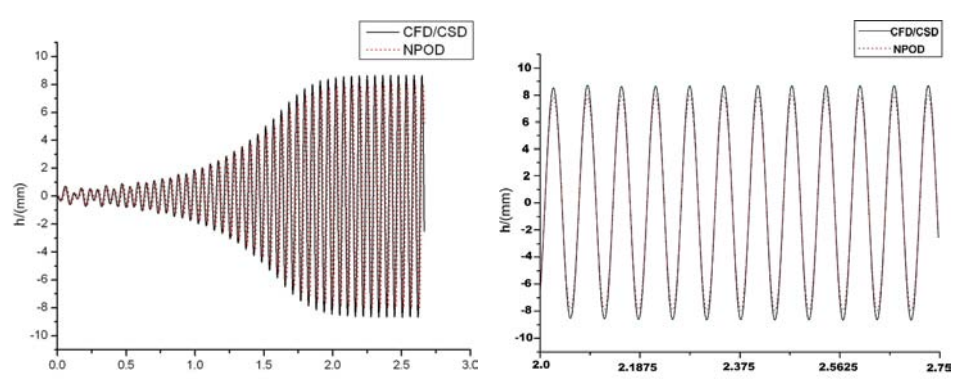

Fig. 4. Plunge movement predicted by NPOD vs. CFD/CSD solver.

also similar to the results simulated by the CFD/CSD couple solver including the position and frequency of the shock.

As same as the traditional POD/ROM, the computation efficiency of NPOD/ROM is also excellent. For LCO prediction of the two-dimensional viscous NLR 7301 aeroelastic model, the computation cost is reduced from the order of hours for direct CFD/CSD solver to on the order of seconds for NPOD/ROM. We can also find out that the NPOD/ROM can predict the response very well even at $\alpha = 3.5°$, which is far from the steady background flow at $\alpha = 0°$ where the ROM is constructed, while the traditional POD/ROM cannot do that. It means that the NPOD/ROM is much more robust to flow parameter variation than traditional POD/ROM. This is on behalf of the second-order items of the dynamically nonlinear snapshots equation.

4.4. *LCO trend prediction*

In this section, the NPOD/ROM is constructed at the condition $\mathrm{Ma} = 0.75$, $\alpha = 0.2°$. And then, we compute the pitch amplitude of LCO trend in different reduced order velocity. Figure 5 gives the LCO pitch amplitude vs. reduced velocity predicted by different models. As it can be seen, the first-order HB/POD can capture LCO very well in some instances such as the reduced velocity 0.37–0.41, but there are still great large errors in other conditions [Thomas *et al.* (2008)]. However, the LCO trend predicted by NPOD/ROM is very closely to the CFD/CSD solver in most instances. It indicates again that NPOD/ROM is a great enhancement to the traditional first-order POD/ROM when the flow state is far away from the steady background flow such as LCO comes out.

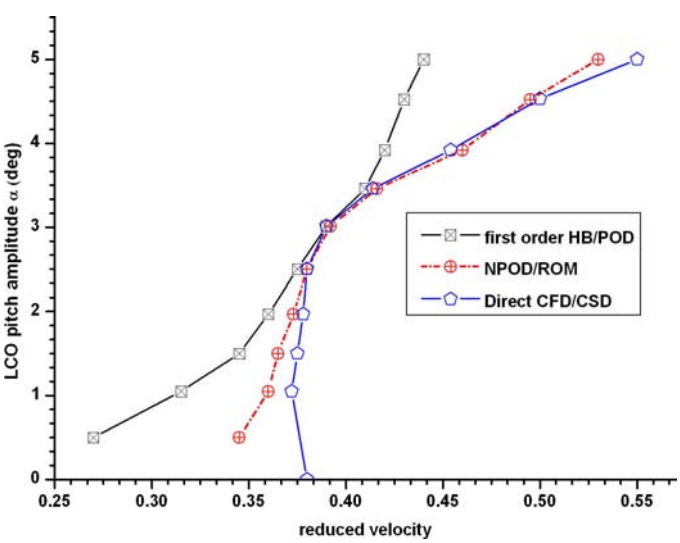

Fig. 5. LCO response trend by different models.

4.5. *Active control for LCO*

LCO is very dangerous for the aircraft structures. Active stability augmentation system is an attractive and promising technology to suppress flutter and LCO. In order to design a good control law, the control plant model with low order and high accuracy must be provided. From the above discussion, the NPOD/ROM had been proved as a good low-order model for representing the nonlinear dynamics. In this section, we will demonstrate the performance of active control law designed based on NPOD/ROM. As Fig. 6, the rear flap of the airfoil can be used as an actuator to stabilize the LCO. We can design the active control law for LCO based on the NPOD/ROM or the Eq. (16) directly. The flux state $\mathbf{w}_r$ cannot be measured directly by the sensors, while the structure movement state variables u and v or the outputs of the aeroelastic system can be measured directly. Equation (16) is a nonlinear system, so the static output feedback linearization method was used to design the control law for stabilizing the nonlinear system [Riccardo and Patrizio (1996)].

In the simulation, the flow condition is as the same as the Sec. 4.3, the time steps is 0.001 second. The controller will start after the aeroelastic system run into LCO at the 7300 time steps. Figures 7 and 8 are the responses of pitch and plunge

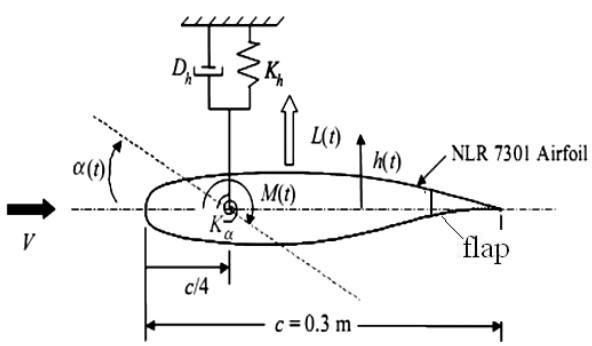

Fig. 6. Typical aeroelastic model with flap.

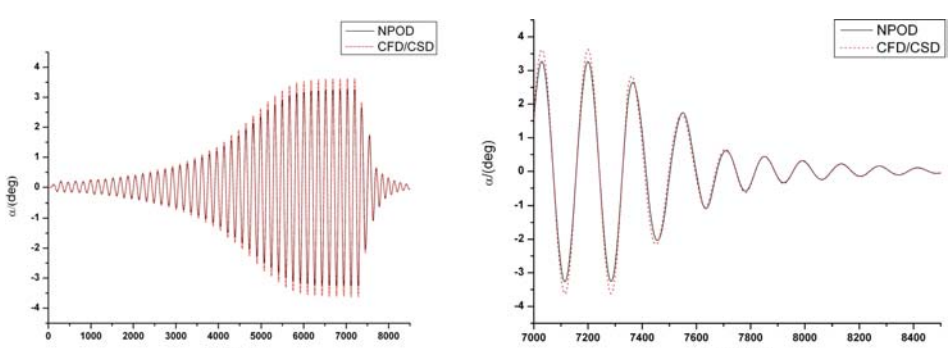

Fig. 7. The response of pitch movement with controller (NPOD vs. CFD/CSD).

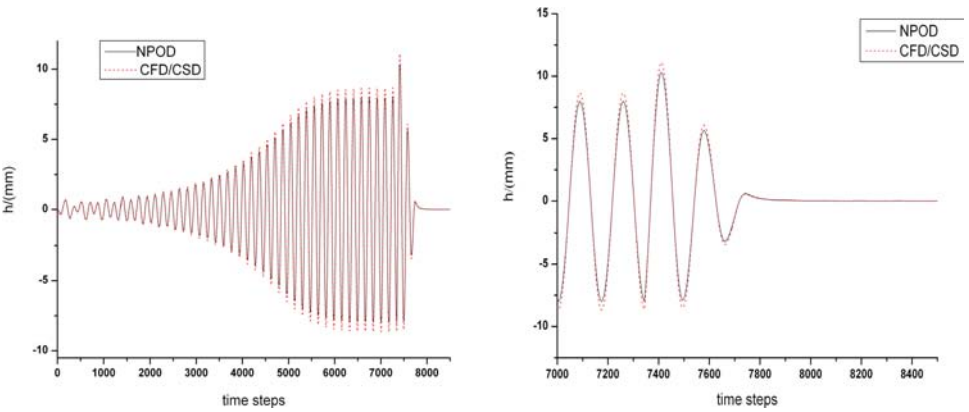

Fig. 8. The response of plunge movement with controller (NPOD vs. CFD/CSD).

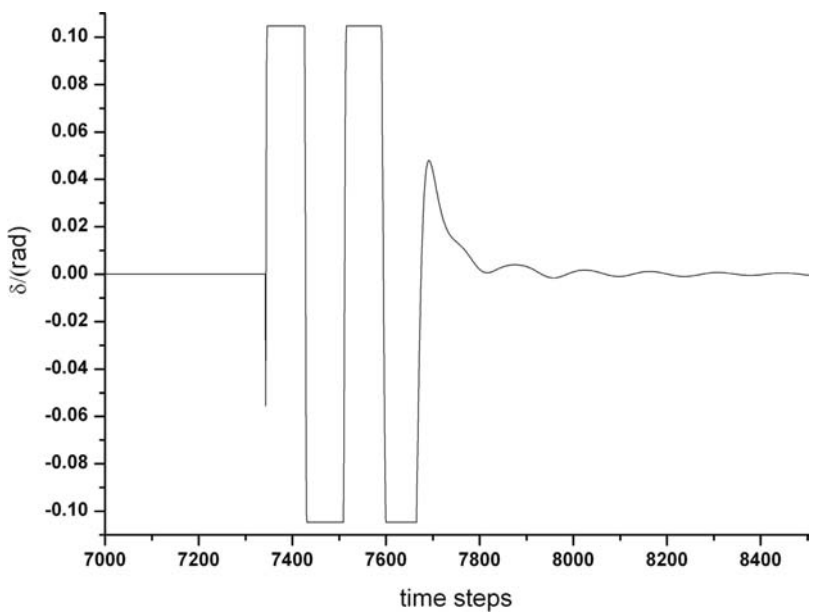

Fig. 9. The response of the flap control.

movement predicted by the NPOD/ROM and CFD/CSD couple solver. Figure 9 is the response of the flap where the largest deflection is limited below 0.1. It can be seen that the LCO can be stabilized very quickly. The results from the two models are very approximate and the NPOD/ROM itself can be used to design and evaluate the control law for LCO directly, while the traditional POD/ROM must combined with the CFD/CSD couple solver to evaluate the robustness of the controller because of linear ROM's poor performance in LCO prediction

[Chen *et al.* (2010)]. It indicates that the NPOD/ROM is good enhancement for active control law design and evaluation and will reduce the design cost and improve the performance of the active controller.

5. Conclusion

The NPOD/ROM, a new nonlinear ROM in time domain for computational fluid dynamic flow solver is investigated. The construction method of NPOD/ROM for aeroelastic system is obtained by the Taylor series expansion of the flow solver together with POD method. The efficiency and capability for NPOD/ROM to predict the LCO is demonstrated by the NRL 7301 aeroelastic experimental model. The simulation results show that the NPOD/ROM can predict the aeroelastic response very well even in the condition some far from the steady background flow where the ROM is constructed with excellent computation efficiency. The other merit is that the active controller of LCO can be directly designed and evaluated without CFD/CSD couple solver. The next step is to extend the NPOD/ROM to model the cases with more flow parameters variation individually or simultaneously such as Mach number, angel of attack, or bank, etc.

Acknowledgment

This work was supported by the National Natural Science Foundation of China (10902082), the Fundamental Research Funds for the Central Universities (xjj20100126), and New Faculty Research Foundation of XJTU.

References

Badcock, K. J. and Woodgate, M. A. [2007] Fast prediction of transonic aeroelastic stability and limit cycles, *AIAA J.* **45**(6), 1370–1381.

Chen, G., Li, Y. M. and Patrick, H. [2010] Design of Active Control Law for Aeroelastic System Based on Proper Orthogonal Decomposition Reduced Order Model, AIAA-2010-2624.

Dietz, G., Schewe, G. and Mai, H. [2004] Experiments on heave/pitch limit-cycle oscillations of a supercritical airfoil close to the transonic dip, *J. Fluids Structures* **19**(1), 1–16.

Dowell, E., Edwards, J. and Strganac, T. [2003] Nonlinear aeroelasticity, *J. Aircraft* **40**(5), 857–874.

Dowell, E. H., Thomas, J. P. and Hall, K. C. [2004] Transonic limit cycle oscillation analysis using reduced order aerodynamic models, *J. Fluids Structures* **19**(1), 17–27.

Hu, G. and Dowell, E. H. [2008] Physics-based identification, modeling and management infrastructure for aeroelastic limit-cycle oscillations, US Air Force Annual Structural Dynamics Conference, Arlington, VA, June 2008.

Lai, K. L. and Tsai, H. M. [2008] Reduced-order based flutter analysis for complex aeroelastic systems, AIAA-2008-6240.

Lieu, T., Farhat, C. and Lesoinne, M. [2006] Reduced-order fluid/structure modeling of a complete aircraft configuration, *Comp. Methods Appl. Mech. Eng.* **195**, 5730–5742.

Lucia, D. J., Beran, P. S. and Silva, W. A. [2004] Reduced-order modeling: New approaches for computational physics, *Prog. Aerospace Sci.* **40**(1), 51–117.

Riccardo, M. and Patrizio, T. [1996] *Nonlinear Control Design: Geometric, Adaptive and Robust*, First Edition, Pearson Education Limited, Italy.

Thomas, J. P., Dowell, E. H. and Hall, K. C. [2003] Three-dimensional transonic aeroelasticity using proper orthogonal decomposition-based reduced order models, *J. Aircraft* **40**(3), 544–551.

Thomas, J. P., Dowell, E. H. and Hall, K. C. [2004] Modeling limit cycle oscillations for an NLR 7301 airfoil aeroelastic configuration including correlation with experiment, *J. Aircraft* **41**(6), 1266–1274.

Thomas, J. P., Dowell, E. H. and Hall, K. C. [2004] Modeling viscous transonic limit cycle oscillation behavior using a harmonic balance approach, *J. Aircraft* **41**(6), 1266–1274.

Thomas, J. P., Dowell, E. H. and Hall, K. C. [2008] Using automatic differentiation to create a nonlinear reduced order model of a computational fluid dynamic solver, AIAA-2008-2322.